Nanoscale Advances

ROYAL SOCIETY OF CHEMISTRY

PAPER

View Article Online
View Journal | View Issue

Cite this: *Nanoscale Adv.*, 2024, **6**, 638

Synergistic effect of composition gradient and morphology on the catalytic activity of amorphous FeCoNi-LDH†

Yuan-Yuan Li, *[ae] Xiao Nan Fu,[a] Lin Zhu,[a] Ying Xie,[a] Gong Lei Shao,[b] Bing-Xin Zhou,[c] Wei-Qing Huang,[d] Gui-Fang Huang[d] and Na Wang[a]

The rational design of electrocatalysts with well-designed compositions and structures for the oxygen evolution reaction (OER) is promising and challenging. Herein, we developed a novel strategy – a one-step double-cation etching sedimentation equilibrium strategy – to synthesize amorphous hollow Fe-Co-Ni layered double hydroxide nanocages with an outer surface of vertically interconnected ultrathin nanosheets (Fe-Co-Ni-LDH), which primarily depends on the *in situ* etching sedimentation equilibrium of the template interface. This unique vertical nanosheet-shell hierarchical nanostructure possesses enhanced charge transfer, increased active sites, and favorable kinetics during electrolysis, resulting in superb electrocatalytic performance for the oxygen evolution reaction (OER). Specifically, the Fe-Co-Ni-LDH nanocages exhibited remarkable OER activity in alkaline electrolytes and achieved a current density of 100 mA cm^{-2} at a low overpotential of 272 mV with excellent stability. This powerful strategy provides a profound molecular-level insight into the control of the morphology and composition of 2D layered materials.

Received 1st November 2023
Accepted 22nd December 2023

DOI: 10.1039/d3na00949a

rsc.li/nanoscale-advances

1. Introduction

The oxygen evolution reaction (OER) is important in various energy storage and conversion systems, such as water splitting devices and metal–air batteries.[1–4] However, its sluggish kinetics owing to the intrinsic four-step proton-coupled electron transfer process is regarded as the bottleneck in the development of these technologies.[5–9] Although Ir- and Ru-based catalysts are the most efficient OER electrocatalysts, their large-scale application has prodigiously suffered from their high cost and scarcity.[10,11] Therefore, exploring non-noble metal OER catalysts with high activity, excellent stability, low cost, and feasible operation is particularly essential for developing energy conversion technologies.[12–17]

First-row transition-metal oxides, hydroxides, sulfides, nitrides, and phosphides exhibit great potential for OER in view of their earth abundance and high catalytic activity.[18–23] Among them, Fe-Ni-Co layered double hydroxide (LDH) is currently deemed to be the most promising OER catalyst in alkaline solution owing to the visibly enhanced catalytic activity, which is derived from the synergistic interactions between Ni, Co, and Fe species.[24–28] As is well known, active sites for the OER catalytic process are principally located on the surface of the catalyst and have a positive influence on the catalytic performance of materials.[29–32] Therefore, the delicate engineering of nanostructures for Ni-Co-Fe LDH-based electrocatalysts by increasing the number of their exposed active sites is of significant importance in enhancing their OER performance.

Hollow nanostructures have displayed distinct advantages as OER catalysts owing to their structure-dependent features, such as a large surface area, multiple interfaces, and short distances for the transfer of charges.[33–37] Compared with smooth-faced hollow structures, nanocages assembled with ultrathin nanosheets possessing large surface area and short diffusion distance for mass transport exhibit apparent superiority in catalysis.[38–40] As a representative method, hard templating has been demonstrated to be effective for the fabrication of complex hollow structures. However, the tedious and complex synthetic procedure makes it inconvenient and unfavorable for the practical application of complex hollow catalysts.[41–43] Most recently, a cation-exchange synthetic approach, which provides easy control for the fabrication of well-defined hollow

[a]*School of Sciences, Henan University of Technology, Zhengzhou 450001, China. E-mail: 85liyuanyuan@haut.edu.cn*

[b]*Interdisciplinary Research Center for Sustainable Energy Science and Engineering (IRC4SE2), School of Chemical Engineering, Zhengzhou University, Zhengzhou 450001, China*

[c]*School of Materials Science and Engineering, Henan Polytechnic University, Jiaozuo 454003, China*

[d]*Department of Applied Physics, School of Physics and Electronics, Hunan University, Changsha 410082, China*

[e]*Institute of Physical Properties for Quantum Functional Materials, School of Sciences, Henan University of Technology, Zhengzhou 450001, China*

† Electronic supplementary information (ESI) available. See DOI: https://doi.org/10.1039/d3na00949a

structures, has been used as a self-templating method to tune the dimensionality and morphology of materials.[9,44,45] Ordered hollow LDH structures have been synthesized by a cation-exchange method using metal–organic framework precursors as starting materials. However, the preparation of multi-metal LDH-based nanocages as electrocatalysts is realized by methods including hydrothermal and multi-step synthesis, which have inherent limitations, including high cost and being time-consuming. Therefore, a facile one-pot self-templating approach is highly desirable for the preparation of novel multi-metal LDH structures catalysts from a metal–organic framework.

Here, we present a facile one-pot double-cation etching strategy to synthesize Fe-Co-Ni-LDH hierarchical nanocages assembled by ultrathin nanosheets. Transforming from the plate-like structure of Co-MOF (a metal–organic framework), hollow hierarchical Fe-Co-Ni-LDH nanocages are obtained through the simultaneous etching and coprecipitation reactions in a double cation salt solution. By adjusting the quality ratio between the two metallic salts, the density of ultrathin nanosheets on the nanocages could be further tailored. The hierarchically hollow superstructures with excellent accessibility and optimized chemical composition make Fe-Co-Ni-LDH nanocages with significantly enhanced electrocatalytic activity toward OER. The new synthetic strategy opens a new way to design highly stable and active OER electrocatalysts.

2. Experimental section

2.1. Fabrication of the crystals

2.1.1. Synthesis of Co-MOF crystals. The cobalt-based metal–organic framework supported on nickel foam (Co-MOF) was synthesized using a previously reported method.[46] Two solutions were prepared by dissolving 0.291 g of $Co(NO_3)_2 \cdot 6H_2O$ and 0.6586 g of 2-methylimidazole in 20 mL of deionized water. The 2-methylimidazole solution was quickly mixed with the $Co(NO_3)_2 \cdot 6H_2O$ solution, after which a piece of clean NF (2.5×3.5 cm^2) was immersed into the mixture solution. The resultant mixture was placed at rest at room temperature for 4 hours. Finally, the as-obtained Co-MOF crystals were cleaned with deionized water, and vacuum dried overnight.

2.1.2. Synthesis of hollow Fe-Co-Ni-LDH nanocages. The as-fabricated Co-MOF was immersed in 20 mL of deionized water solution containing 100 mg of urea, 50 mg of $FeSO_4 \cdot 7H_2O$, and 150 mg of $Ni(NO_3)_2 \cdot 6H_2O$. After the reaction for 20 min at 70 °C using an oil bath, the resulting product was washed with ethyl alcohol and deionized water at least three times, and then dried at 60 °C to provide a Fe-Co-Ni-LDH sample. Similarly, the Fe-Co-Ni-LDH samples obtained with different $FeSO_4 \cdot 7H_2O$ content (25, 50, 75, 100, and 150 mg were denoted as Fe-Co-Ni-LDH-1, Fe-Co-Ni-LDH-2, Fe-Co-Ni-LDH-3, Fe-Co-Ni-LDH-4 and Fe-Co-Ni-LDH-5, respectively).

2.1.3. Synthesis of hollow Ni-Co-LDH nanocages. Hollow Ni-Co-LDH nanocages were prepared by a similar process of Fe-Co-Ni-LDH by adding only urea and $Ni(NO_3)_2 \cdot 6H_2O$.

2.1.4. Synthesis of the Fe-Co-LDH nanosheets. Fe-Co-LDH nanosheets were prepared by a similar process of Fe-Co-Ni-LDH by adding only urea and $FeSO_4 \cdot 7H_2O$. Similarly, Co-Fe-LDH samples obtained with different $FeSO_4 \cdot 7H_2O$ contents (50, 100, and 150 mg were denoted as Fe-Co-LDH-2, Fe-Co-LDH-4, and Fe-Co-LDH-5, respectively).

2.2. Characterization

The morphologies of samples were evaluated using SEM (Hitachi S-4800). X-ray powder diffraction (XRD) patterns were obtained on an X-ray diffractometer at 40 kV and 40 mA with Cu Kα radiation. X-ray photoelectron spectroscopy (XPS) was recorded using a model of Thermo Scientific Escalab 250Xi spectrometer.

2.3. Electrochemical measurement

The electrocatalytic activities of the catalysts (1×1 cm^2) for the oxygen evolution reaction (OER) were studied at room temperature using a standard three-electrode system in the 1.0 M KOH aqueous electrolyte. A saturated Ag/AgCl electrode and Pt plate were used as reference and counter electrodes, respectively. The polarization curves were measured at 2 mV s^{-1} and *iR* corrected, and all potentials measured were calibrated to a reversible hydrogen electrode (RHE) using the following equation: $E_{RHE} = E_{Ag/AgCl} + 0.197 + 0.059 \times pH$. Overpotential ($\eta$) was calculated using the following formula: η (V) $= E_{RHE} - 1.23$ V. Electrochemical impedance spectroscopy (EIS) was performed in a frequency range of 0.01 Hz and 1000 kHz.

3. Results and discussion

3.1. Morphology and microstructure of the hollow Fe-Co-Ni-LDH nanocages

The uniform hierarchical triangular Fe-Co-Ni-LDH nanocages were prepared *via* the dication-exchange self-templating strategy as depicted schematically in Fig. 1. First, uniform plate-like Co-MOF with smooth surfaces growing on the NF were synthesized as the sacrificial templates (Fig. 2a). After the hydrolysis reactions of urea, nickel nitrate, and ferrous sulfate in a solution of water, hierarchical triangular Fe-Co-Ni-LDH nanocages were obtained. During this formation process, Co-MOF templates can be gradually etched with the hydrolyzation reactions, and the released Co species were coprecipitated with Fe^{2+}, Ni^{2+}, and OH^- ions to form thin layered Fe-Co-Ni-LDH nanocages.[18] Meanwhile, Ni-Co-LDH and Fe-Co-LDH are also prepared for comparison. Notably, the distinctly different morphology between Fe-Co-Ni-LDH, Co-Ni-LDH, and Fe-Co-LDH can be observed (Fig. 2). Compared with the Fe-Co-Ni-LDH nanocages (Fig. 2f–j), the Fe-Co-LDH exhibits the nanosheet structure (Fig. 2e), which may be attributed to the faster etching rates than the coprecipitation rates. Interestingly, as nickel nitrate is introduced, the morphology of Fe-Co-Ni-LDH forms trigonal nanocages with ultra-thin folded nanosheets. This morphology change suggests that the nickel nitrate can slow down the etching rate. The Fe-Co-Ni-LDH morphology can be steadily controlled by adjusting the etching and coprecipitation rates by controlling the ratio of the two metal salts. Specifically, more ferrous sulfate in the mixed solvent speeds up

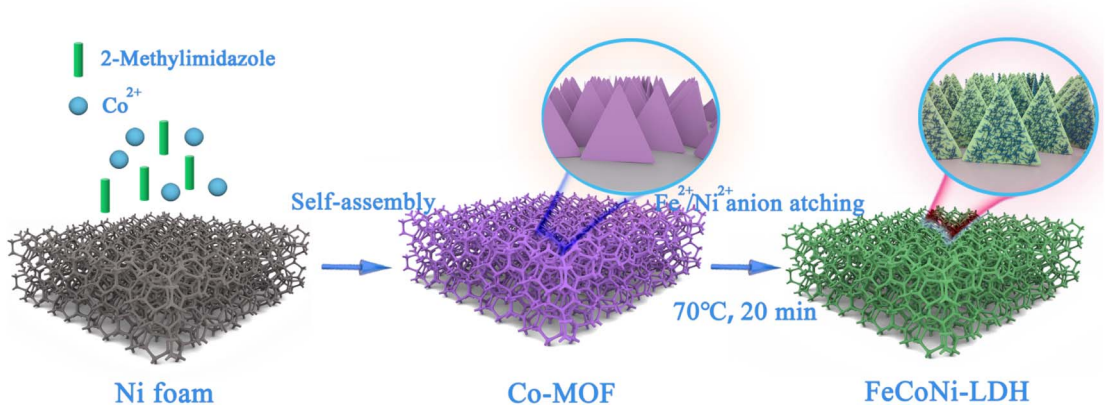

Fig. 1 The preparation of hollow Fe-Co-Ni-LDH nanocages. The uniform hierarchical triangular Fe-Co-Ni-LDH nanocages are prepared *via* the dication-exchange self-templating strategy.

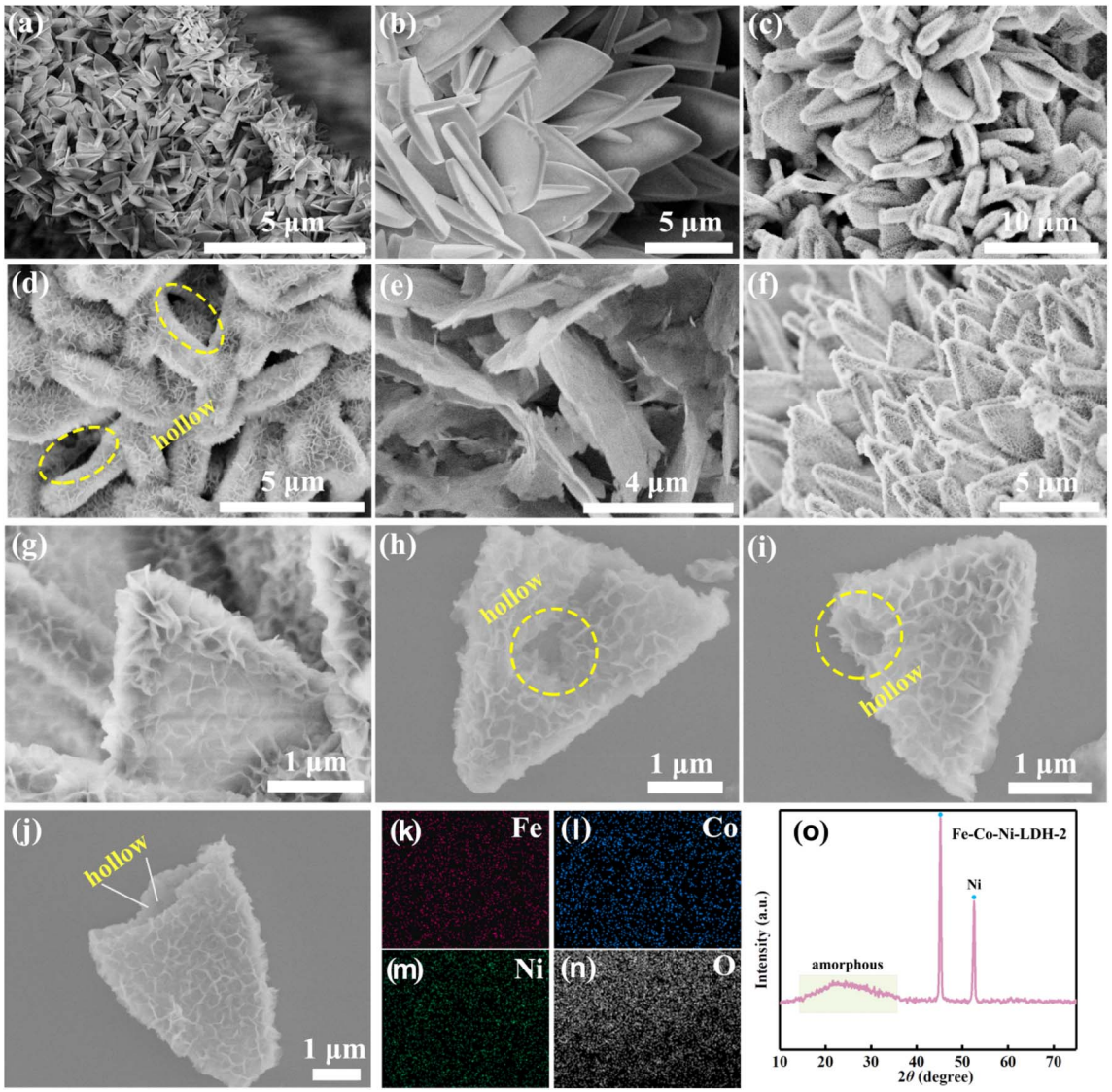

Fig. 2 Morphology control of hollow Fe-Co-Ni-LDH nanocages. SEM images of (a and b) Co-MOF, (c and d) Ni-Co-LDH, (e) Fe-Co-LDH, and (f–j) Fe-Co-Ni-LDH-2. (k–n) SEM-EDS elemental mapping of Fe-Co-Ni-LDH-2. (o) XRD patterns of Fe-Co-Ni-LDH-2.

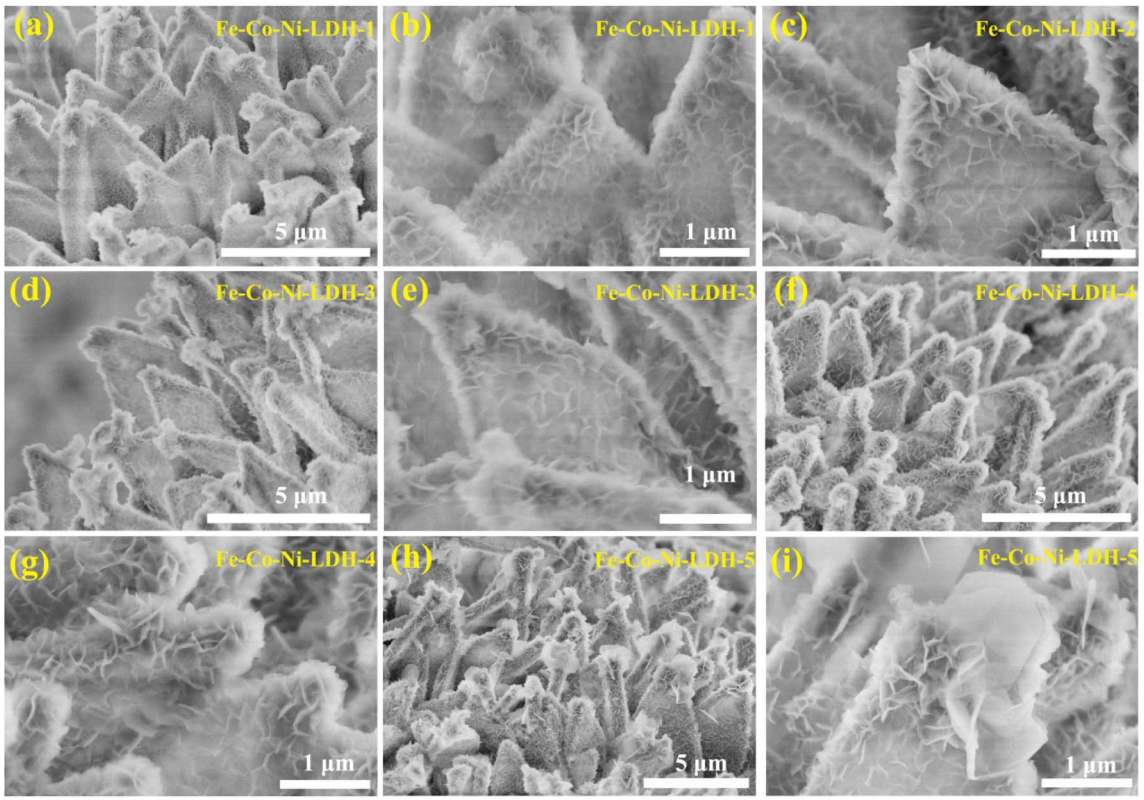

Fig. 3 SEM images of (a and b) Fe-Co-Ni-LDH-1, (c) Fe-Co-Ni-LDH-2, (d and e) Fe-Co-Ni-LDH-3, (f and g) Fe-Co-Ni-LDH-4, and (h and i) Fe-Co-Ni-LDH-5.

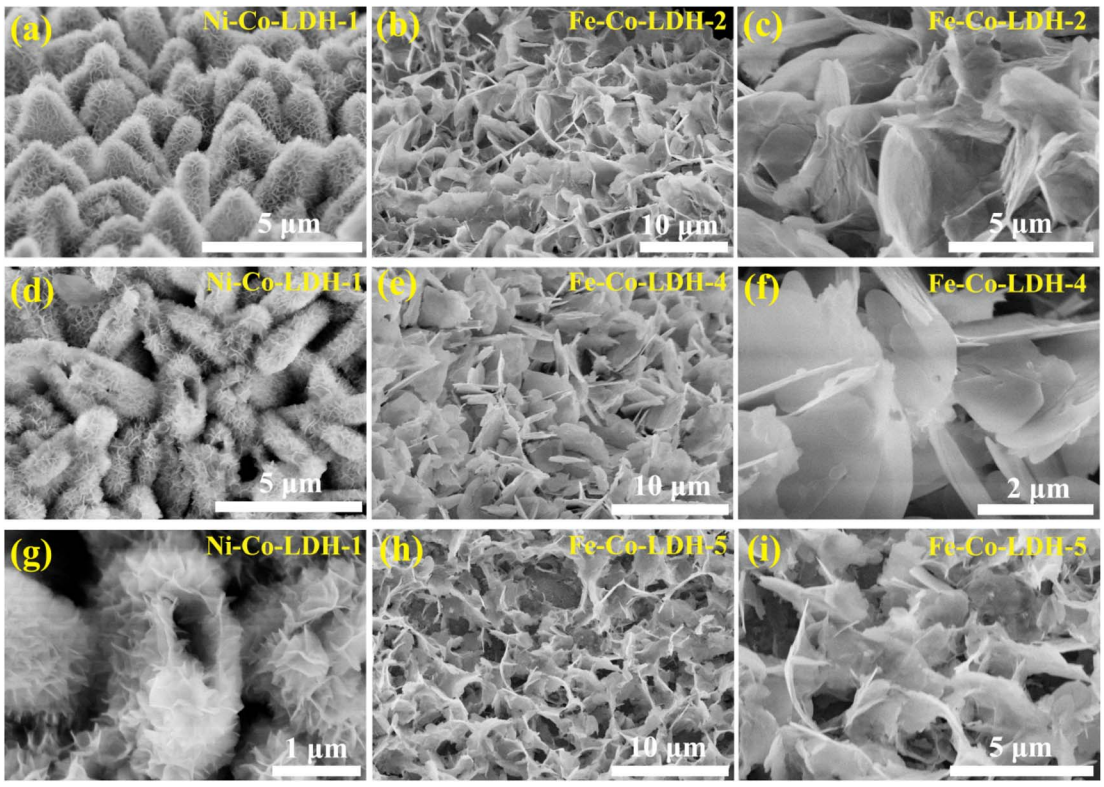

Fig. 4 SEM images of (a, d, and g) Ni-Co-LDH-1, (b and c) Fe-Co -LDH-2, (e and f) Fe-Co -LDH-4, and (h and i) Fe-Co-LDH-5.

the etching of Co-MOF, which could decrease the number of external nanosheets produced on the Fe-Co-Ni-LDH nanocages owing to the fast etching of the template.

To reveal the structure–activity relationship, hollow Fe-Co-Ni-LDH nanocages with interlocked nanosheets were verified by SEM, as displayed in Fig. 1. As the Co-MOF sheet-like arrays (Fig. 2a and b) acted as a sacrificial template for the *in situ* growth of Fe-Co-Ni-LDH, the samples inherited similar sheet-like arrays after the transformation in the presence of $FeSO_4$ and $Ni(NO_3)_2$ (Fig. 2f). Furthermore, it can be observed that the interlocked nanosheets were vertically standing in the whole hollow skeleton rather uniformly, creating abundant straight channels and pathways (Fig. 2g–j), obviously different from the Fe-Co-LDH single nanosheet structure (Fig. 2e). Notably, SEM (Fig. 2c and d) images show that Ni-Co-LDH has a similar nanocage morphology assembled of more high-density ultrathin nanosheets compared with Fe-Co-Ni-LDH, indicating that the addition of ferrous sulfate could accelerate the etching rate. However, as shown below, this decrease does not lead to any drop in the catalytic activity, which is sufficient to identify the positive effect of the introduction of Fe. To investigate the spatial distribution of different elements, elemental mapping analysis in the scanning SEM mode was carried out on Fe-Co-Ni-LDH. The SEM elemental mapping images showed the uniform distribution of Fe, Ni, Co, and O elements (Fig. 2k–n), suggesting the expected high homogeneity of nickel and cobalt hydroxides in this hierarchical micro–nano sheet structure. In the XRD pattern of the sample, there were only two narrow peaks at 45° and 53° assigned to the Ni nickel foam and a broad peak from 15–35° suggesting that the original structure of Fe-Co-Ni-LDH was destroyed and a new amorphous species might have been formed (Fig. 2o).[47,48] This particular morphology, which generally enables high active-site density, could greatly improve the electrocatalysis for the OER. Furthermore, the surface nanosheet density of Fe-Co-Ni-LDH nanocages gradually decreased with increasing mass of ferrous sulfate (Fig. 3). The hollow structures with an outer shell of rich ultrathin nanosheets of Fe-Co-Ni-LDH could not only provide larger specific surface area, more exposed active sites, and better access for electrolytes but also shorter diffusion paths for mass and electrons.[49,50]

The surface elemental composition and chemistry of Fe-Co-Ni-LDH nanocages were investigated *via* X-ray photoelectron spectroscopy (XPS), as shown in Fig. 5. The survey spectra confirmed that both Fe-Co-Ni-LDH samples were mainly comprised Fe, Co, Ni, and O elements. The binding energies of Co 2p at 780.8 and 796.9 eV and the satellite peaks at 785.9 and 802.6 eV can be assigned to Co^{2+} species in Fe-Co-Ni-LDH

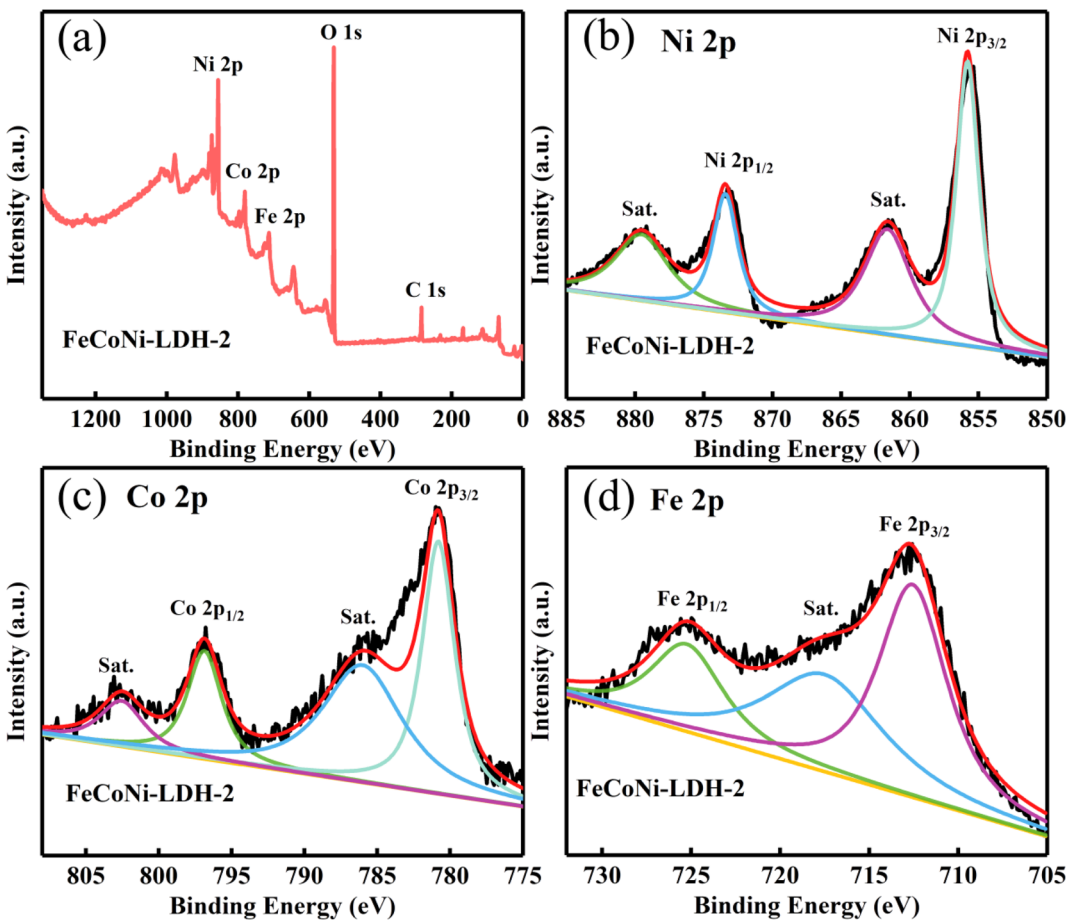

Fig. 5 Microstructure of hollow Fe-Co-Ni-LDH nanocages. (a) XPS, (b) Ni 2p, (c) Co 2p, and (d) Fe 2p spectra of Fe-Co-Ni-LDH-2.

nanocages.[51] The XPS spectra of Ni 2p indicate that the peaks in $2p_{3/2}$ (855.8 eV) and $2p_{1/2}$ (873.5 eV) regions with two shake up satellite peaks at 861.5 and 879.6 eV are related to the presence of Ni^{2+} species (Fig. 5b).[52] The Fe species of the sample are found to be mostly in the +3 oxidation state according to the high-resolution XPS spectra of Fe 2p (Fig. 5d).[24] The above results prove the introduction of the Fe element.

3.2. Relationship between component and morphology of Fe-Co-Ni-LDH electrocatalytic oxygen evolution

To elucidate the effect of the optimization on catalysis in general, the OER activities of Fe-Co-Ni-LDH nanocages were studied using a three-electrode system in an alkaline solution (1.0 m KOH) at a scan rate of 2 mV s^{-1}. The electrocatalytic properties of Fe-Co-Ni-LDH, Ni-Co-LDH, Fe-Co-LDH, Ir/C, and NF were also studied as references. Fig. 6a shows the *iR*-compensated linear sweep voltammetry (LSV) curves of the samples. One can see that the Fe-Co-Ni-LDH nanocages catalyst showed a remarkably higher current density than the Ni-Co LDH with a high C_{dl}, Fe-Co LDH, Ir/C, and NF samples at the same η. To reach a current density of 50 mA cm^{-2}, the Fe-Co-Ni-LDH nanocages catalyst required an η of only 246 mV, which is 122 mV lower than that of Ni-Co-LDH (Fig. 6b). Moreover, the OER kinetics of Fe-Co-Ni-LDH is much faster than that of Ni-Co LDH. Specifically, the current density of Fe-Co-Ni-LDH could reach 100 mA cm^{-2} at the η of 272 mV, which is 133 mV lower than that of Ni-Co LDH (Fig. 4b). As shown in Fig. 6c, the catalytic kinetics of all samples were assessed using Tafel plots. A smaller Tafel slope was observed for Fe-Co-Ni-LDH compared to that of Ni-Co-LDH, Fe-Co-LDH, Ir/C, and NF. The Fe-Co-Ni-LDH nanocages exhibited a low Tafel slope of 77.8 mV dec^{-1}, which was much smaller than that of Ni-Co-LDH nanocages (111.5 mV dec^{-1}). The OER performance of the as-prepared Fe-Co-Ni-LDH was compared with those of the other reported LDH-based electrocatalysts, as listed in Table S1.† It can be found that the OER activities of the hollow Fe-Co-Ni-LDH electrocatalysts were better than those reported for most LDH-based electrocatalysts (Table S1†). The enhanced activity of Fe-Co-Ni-LDH-2 nanocages can be largely attributed to the increased electrochemically active surface area and the decreased transfer resistance owing to the fine-tuning of the electronic structure.[53] Moreover, the Fe-Co-Ni-LDH samples developed higher OER catalytic activity with increasing $FeSO_4$ (Fig. 4d). Upon increasing the $FeSO_4$ content to 75 mg, the OER catalytic activity of Fe-Co-Ni-LDH remained unchanged, indicating that the enhanced activity was due to the combined effect of the morphology regulation and the electronic structure change. Furthermore, a relatively stable current density was observed at a scan rate of 50 mV s^{-1} during the durability test, indicating

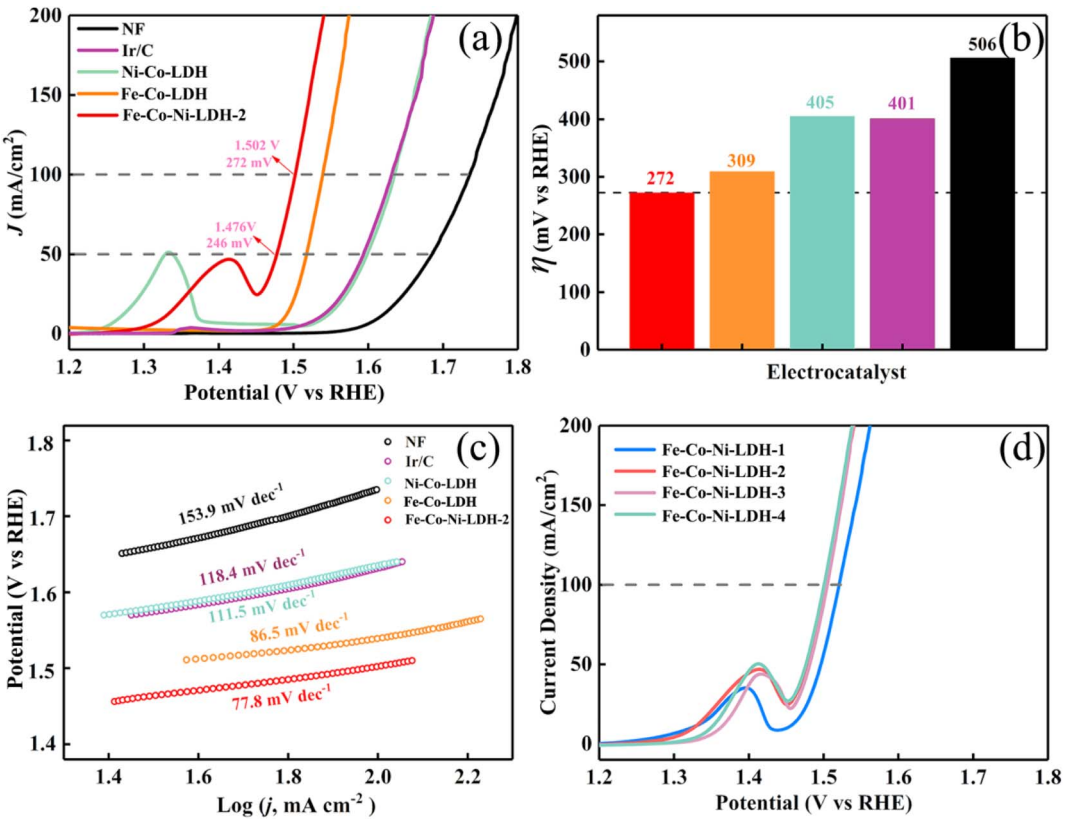

Fig. 6 The OER activity of hollow Fe-Co-Ni-LDH nanocages. (a) Linear sweep voltammetry curves, (b) comparison of OER activity of the samples at a current density of 50 mA cm^{-2}, and (c) Tafel plots of the electrocatalysts in 1.0 M KOH solution of NF, Ir/C, Ni-Co-LDH, Fe-Co-LDH and Fe-Co-Ni-LDH. (d) Linear sweep voltammetry curves of Fe-Co-Ni-LDH-1, Fe-Co-Ni-LDH-2, Fe-Co-Ni-LDH-3, and Fe-Co-Ni-LDH-4.

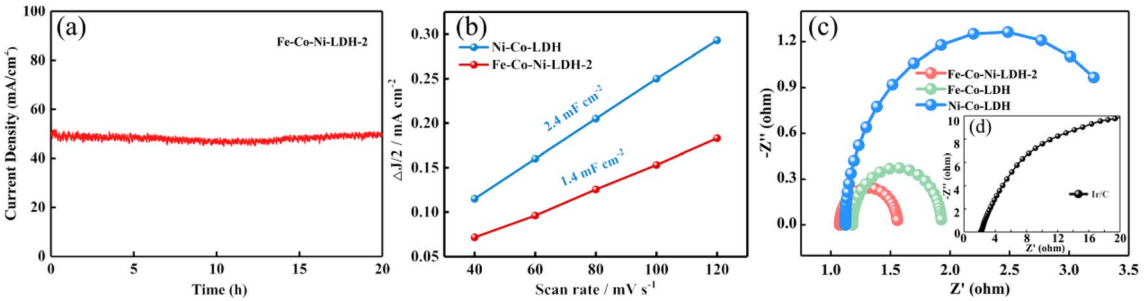

Fig. 7 (a) Time-dependent current density curves of Fe-Co-Ni-LDH-2. (b) The electrochemical surface areas of Ni-Co-LDH and Fe-Co-Ni-LDH-2. (c) Nyquist plots of impedance spectroscopy analysis of Ni-Co-LDH, Fe-Co-LDH, and Fe-Co-Ni-LDH-2. (d) Nyquist plots of impedance spectroscopy analysis of the Ir/C sample.

the excellent long-term operating stability of Fe-Co-Ni-LDH (Fig. 7a). These results show the high OER durability of Fe-Co-Ni-LDH nanocage catalysts.

3.3. OER enhancement mechanism of Fe-Co-Ni-LDH

To investigate the possible reason for the enhanced electrocatalytic activity of Fe-Co-Ni-LDH, the electrochemically active surface area (ECSA) measurements were carried out using the CV method in the non-faradic region at different scan rates. As shown in Fig. 7b, the C_{dl} values of Ni-Co-LDH and Fe-Co-Ni LDH were 2.4 and 1.4 mF cm^{-2}, respectively. The C_{dl} of Ni-Co-LDH (2.4 mF cm^{-2}) is higher than that of Fe-Co-Ni LDH (1.4 mF cm^{-2}), suggesting that more active sites are exposed in Ni-Co-LDH since C_{dl} is usually applied as the indicator of electrochemically active surface area.[54] However, Fe-Co-Ni LDH catalysts have better catalytic performance than Ni-Co-LDH catalysts. This result indicates that catalytic activity is not only determined by the abundance of the active sites. To further understand the explanations for the enhanced activity of Fe-Co-Ni LDH, the electrochemical impedance spectroscopy characterizations are shown in Fig. 7c and d. It is noteworthy that Fe-Co-Ni-LDH nanocages showed a much smaller semicircle in comparison with Fe-Co-LDH, Ni-Co-LDH, and Ir/C suggesting its lower resistance for faster charge-transfer kinetics,[55] which could be caused by the hollow structure and Fe element implantation. Supporting the above results, it is deduced that Fe-Co-Ni-LDH provided an excellent electrochemical activity for enhanced charge transfer, more active sites, and favorable kinetics during electrolysis by the synergistic effect of composition gradient and morphology. Benefiting from these features, Fe-Co-Ni-LDH demonstrated outstanding capacity for the oxygen evolution reaction.

4. Conclusions

In summary, the amorphous hierarchical hollow Fe-Co-Ni-LDH C-doped CN nanocages with ultrathin nanosheets were designed and fabricated by a novel one-step double cation etching strategy with high-efficiency electrocatalytic oxygen evolution reaction, compared to Co-Ni-LDH nanocages, among the best reported non-precious OER electrocatalysts. This strategy ensures the controllable conversion of Co-MOF precursors into a series of hollow Fe-Co-Ni-LDH nanostructures with tunable structural topology as well as components. The improved activity of the Fe-Co-Ni-LDH nanocages is owing to the increased intrinsic activity, decreased transfer resistance, and more exposed active sites. The double-cation etching strategy proposed here sheds light on the importance of controlling the structure and composition of high-efficiency electrocatalysts for the energy and environment-associated applications.

Conflicts of interest

There are no conflicts to declare.

Acknowledgements

The authors are grateful to the Science Foundation of Henan University of Technology (2018BS058) and the Innovative Funds Plan of Henan University of Technology (2022ZKCJ10).

References

1 J. Suntivich, K. J. May, H. A. Gasteiger, J. B. Goodenough and Y. Shao-Horn, A Perovskite Oxide Optimized for Oxygen Evolution Catalysis from Molecular Orbital Principles, *Science*, 2011, **334**, 1383–1385.
2 T. Wu, S. Sun, J. Song, S. Xi, Y. Du, B. Chen, W. A. Sasangka, H. Liao, C. L. Gan, G. G. Scherer, L. Zeng, H. Wang, H. Li, A. Grimaud and Z. J. Xu, Iron-facilitated dynamic active-site generation on spinel $CoAl_2O_4$ with self-termination of surface reconstruction for water oxidation, *Nat. Catal.*, 2019, **2**, 763–772.
3 A. Grimaud, W. T. Hong, Y. Shao-Horn and J. M. Tarascon, Anionic redox processes for electrochemical devices, *Nat. Mater.*, 2016, **15**, 121–126.
4 F. Li, G.-F. Han, J.-P. Jeon, T. J. Shin, Z. Fu, Y. Lu and J.-B. Baek, Surface Electronic Modulation with Hetero-Single Atoms to Enhance Oxygen Evolution Catalysis, *ACS Nano*, 2021, **15**, 11891–11897.
5 W. T. Hong, M. Risch, K. A. Stoerzinger, A. Grimaud, J. Suntivich and Y. Shao-Horn, Toward the rational design

of non-precious transition metal oxides for oxygen electrocatalysis, *Energy Environ. Sci.*, 2015, **8**, 1404–1427.

6 E. Fabbri, M. Nachtegaal, T. Binninger, X. Cheng, B.-J. Kim, J. Durst, F. Bozza, T. Graule, R. Schaublin, L. Wiles, M. Pertoso, N. Danilovic, K. E. Ayers and T. J. Schmidt, Dynamic surface self-reconstruction is the key of highly active perovskite nano-electrocatalysts for water splitting, *Nat. Mater.*, 2017, **16**, 925–932.

7 H. Zhang, W. Zhou, J. Dong, X. F. Lu and X. W. Lou, Intramolecular electronic coupling in porous iron cobalt (oxy)phosphide nanoboxes enhances the electrocatalytic activity for oxygen evolution, *Energy Environ. Sci.*, 2019, **12**, 3348–3355.

8 Z.-P. Wu, H. Zhang, S. Zuo, Y. Wang, S. L. Zhang, J. Zhang, S.-Q. Zang and X. W. Lou, Manipulating the Local Coordination and Electronic Structures for Efficient Electrocatalytic Oxygen Evolution, *Adv. Mater.*, 2021, **33**, 2103004.

9 M. Chen, C. Peng, Y. Su, X. Chen, Y. Zhang, Y. Wang, J. Peng, Q. Sun, X. Liu and W. Huang, A General Strategy for Hollow Metal-Phytate Coordination Complex Micropolyhedra Enabled by Cation Exchange, *Angew. Chem., Int. Ed.*, 2020, **59**, 20988–20995.

10 D.-Y. Kuo, J. K. Kawasaki, J. N. Nelson, J. Kloppenburg, G. Hautier, K. M. Shen, D. G. Schlom and J. Suntivich, Influence of Surface Adsorption on the Oxygen Evolution Reaction on IrO_2(110), *J. Am. Chem. Soc.*, 2017, **139**, 3473–3479.

11 B.-J. Kim, D. F. Abbott, X. Cheng, E. Fabbri, M. Nachtegaal, F. Bozza, I. E. Castelli, D. Lebedev, R. Schaeublin, C. Coperet, T. Graule, N. Marzari and T. J. Schmidt, Unraveling Thermodynamics, Stability, and Oxygen Evolution Activity of Strontium Ruthenium Perovskite Oxide, *ACS Catal.*, 2017, **7**, 3245–3256.

12 Z.-P. Wu, X. F. Lu, S.-Q. Zang and X. W. Lou, Non-Noble-Metal-Based Electrocatalysts toward the Oxygen Evolution Reaction, *Adv. Funct. Mater.*, 2020, **30**, 1910274.

13 Y. Jia, L. Zhang, A. Du, G. Gao, J. Chen, X. Yan, C. L. Brown and X. Yao, Defect Graphene as a Trifunctional Catalyst for Electrochemical Reactions, *Adv. Mater.*, 2016, **28**, 9532–9538.

14 L. Sondermann, W. Jiang, M. Shviro, A. Spiess, D. Woschko, L. Rademacher and C. Janiak, Nickel-Based Metal-Organic Frameworks as Electrocatalysts for the Oxygen Evolution Reaction (OER), *Molecules*, 2022, **27**, 1241.

15 R. Zhong, Q. Wang, L. Du, Y. Pu, S. Ye, M. Gu, Z. C. Zhang and L. Huang, Length Ultrathin polycrystalline Co_3O_4 nanosheets with enriched oxygen vacancies for efficient electrochemical oxygen evolution and 5-hydroxymethylfurfural oxidation, *Appl. Surf. Sci.*, 2022, **584**, 152553.

16 X. Sun, S. Wang, Y. Hou, X. F. Lu, J. Zhang and X. Wang, Self-supporting metal-organic framework-based hydrogen and oxygen electrocatalysts, *J. Mater. Chem. A*, 2023, **11**, 13089–13106.

17 B. Wang, T. Wu, G. Chen, X. Liu, W. Li, Q. He, D.-S. Li, B. Y. Guan and Y. Liu, General Synthesis of Hierarchically Macro/Mesoporous Fe,Ni-Doped CoSe/N-Doped Carbon Nanoshells for Enhanced Electrocatalytic Oxygen Evolution, *Inorg. Chem.*, 2021, **60**, 6782–6789.

18 J. Zhang, L. Yu, Y. Chen, X. F. Lu, S. Gao and X. W. Lou, Designed Formation of Double-Shelled Ni-Fe Layered-Double-Hydroxide Nanocages for Efficient Oxygen Evolution Reaction, *Adv. Mater.*, 2020, **32**, 1906432.

19 J. Shan, C. Ye, S. Chen, T. Sun, Y. Jiao, L. Liu, C. Zhu, L. Song, Y. Han, M. Jaroniec, Y. Zhu, Y. Zheng and S.-Z. Qiao, Short-Range Ordered Iridium Single Atoms Integrated into Cobalt Oxide Spinel Structure for Highly Efficient Electrocatalytic Water Oxidation, *J. Am. Chem. Soc.*, 2021, **143**, 5201–5211.

20 Y. Li, Z. Wang, J. Hu, S. Li, Y. Du, X. Han and P. Xu, Metal-Organic Frameworks Derived Interconnected Bimetallic Metaphosphate Nanoarrays for Efficient Electrocatalytic Oxygen Evolution, *Adv. Funct. Mater.*, 2020, **30**, 1910498.

21 L. Zhang, J. Peng, Y. Yuan, W. Zhang and K. Peng, Bifunctional heterostructure NiCo-layered double hydroxide nanosheets/NiCoP nanotubes/Ni foam for overall water splitting, *Appl. Surf. Sci.*, 2021, **557**, 149831.

22 H. Yan, Y. Xie, A. Wu, Z. Cai, L. Wang, C. Tian, X. Zhang and H. Fu, Anion-Modulated HER and OER Activities of 3D Ni-V-Based Interstitial Compound Heterojunctions for High-Efficiency and Stable Overall Water Splitting, *Adv. Mater.*, 2019, **31**, 1901174.

23 H. Yang, L. Gong, H. Wang, C. Dong, J. Wang, K. Qi, H. Liu, X. Guo and B. Y. Xia, Preparation of nickel-iron hydroxides by microorganism corrosion for efficient oxygen evolution, *Nat. Commun.*, 2020, **11**, 5075.

24 X. Zhang, F. Yan, X. Ma, C. Zhu, Y. Wang, Y. Xie, S.-L. Chou, Y. Huang and Y. Chen, Regulation of Morphology and Electronic Structure of FeCoNi Layered Double Hydroxides for Highly Active and Stable Water Oxidization Catalysts, *Adv. Energy Mater.*, 2021, **11**, 2102141.

25 C. Huang, Y. Zhong, J. Chen, J. Li, W. Zhang, J. Zhou, Y. Zhang, L. Yu and Y. Yu, Fe induced nanostructure reorganization and electronic structure modulation over CoNi (oxy)hydroxide nanorod arrays for boosting oxygen evolution reaction, *Chem. Eng. J.*, 2021, **403**, 126304.

26 Y. Jin, G. Xi, R. Li, Z.-A. Li, X.-B. Chen and T. Zhang, Nanoporous metallic-glass electrocatalysts for highly efficient oxygen evolution reaction, *J. Alloys Compd.*, 2021, **852**, 156876.

27 N. H. Kwon, M. Kim, X. Jin, J. Lim, I. Y. Kim, N.-S. Lee, H. Kim and S.-J. Hwang, A rational method to kinetically control the rate-determining step to explore efficient electrocatalysts for the oxygen evolution reaction, *NPG Asia Mater.*, 2018, **10**, 659–669.

28 A.-L. Wang, H. Xu and G.-R. Li, NiCoFe Layered Triple Hydroxides with Porous Structures as High-Performance Electrocatalysts for Overall Water Splitting, *ACS Energy Lett.*, 2016, **1**, 445–453.

29 C. Wang and L. Qi, Heterostructured Inter-Doped Ruthenium-Cobalt Oxide Hollow Nanosheet Arrays for Highly Efficient Overall Water Splitting, *Angew. Chem., Int. Ed.*, 2020, **59**, 17219–17224.

30 K. L. Zhou, C. Wang, Z. Wang, C. B. Han, Q. Zhang, X. Ke, J. Liu and H. Wang, Seamlessly conductive $Co(OH)_2$

tailored atomically dispersed Pt electrocatalyst with a hierarchical nanostructure for an efficient hydrogen evolution reaction, *Energy Environ. Sci.*, 2020, **13**, 3082–3092.

31 E. Hu, J. Ning, D. Zhao, C. Xu, Y. Lin, Y. Zhong, Z. Zhang, Y. Wang and Y. Hu, A Room-Temperature Postsynthetic Ligand Exchange Strategy to Construct Mesoporous Fe-Doped CoP Hollow Triangle Plate Arrays for Efficient Electrocatalytic Water Splitting, *Small*, 2018, **14**, 1704233.

32 S. Pan, B. Li, J. Yu, L. Zhao and Y. Zhang, Composition controllable fabrication of ultrathin 2D CoMn layered double hydroxides for highly efficient electrocatalytic oxygen evolution, *Appl. Surf. Sci.*, 2021, **539**, 148305.

33 U. K. Ghorai, S. Paul, B. Ghorai, A. Adalder, S. Kapse, R. Thapa, A. Nagendra and A. Gain, Scalable Production of Cobalt Phthalocyanine Nanotubes: Efficient and Robust Hollow Electrocatalyst for Ammonia Synthesis at Room Temperature, *ACS Nano*, 2021, **15**, 5230–5239.

34 F. Gong, M. Liu, S. Ye, L. Gong, G. Zeng, L. Xu, X. Zhang, Y. Zhang, L. Zhou, S. Fang and J. Liu, All-pH Stable Sandwich-Structured MoO_2/MoS_2/C Hollow Nanoreactors for Enhanced Electrochemical Hydrogen Evolution, *Adv. Funct. Mater.*, 2021, **31**, 2101715.

35 P. Kuang, Y. Wang, B. Zhu, F. Xia, C.-W. Tung, J. Wu, H. M. Chen and J. Yu, Pt Single Atoms Supported on N-Doped Mesoporous Hollow Carbon Spheres with Enhanced Electrocatalytic H_2-Evolution Activity, *Adv. Mater.*, 2021, **33**, 2008599.

36 Y. Li, S. L. Zhang, W. Cheng, Y. Chen, D. Luan, S. Gao and X. W. Lou, Loading Single-Ni Atoms on Assembled Hollow N-Rich Carbon Plates for Efficient CO_2 Electroreduction, *Adv. Mater.*, 2022, **34**, 2105204.

37 D. D. Boehm, M. Beetz, M. Schuster, K. Peters, A. G. Hufnagel, M. Doeblinger, B. Boeller, T. Bein and D. Fattakhova-Rohlfing, Efficient OER Catalyst with Low Ir Volume Density Obtained by Homogeneous Deposition of Iridium Oxide Nanoparticles on Macroporous Antimony-Doped Tin Oxide Support, *Adv. Funct. Mater.*, 2020, **30**, 1906670.

38 Y. Z. Wang, M. Yang, Y.-M. Ding, N.-W. Li and L. Yu, Recent Advances in Complex Hollow Electrocatalysts for Water Splitting, *Adv. Funct. Mater.*, 2022, **32**, 2108681.

39 H. Li, S. Chen, Y. Zhang, Q. Zhang, X. Jia, Q. Zhang, L. Gu, X. Sun, L. Song and X. Wang, Systematic design of superaerophobic nanotube-array electrode comprised of transition-metal sulfides for overall water splitting, *Nat. Commun.*, 2018, **9**, 2452.

40 L. Li, X. Dai, D.-L. Chen, Y. X. Zeng, Y. Hu and X.-W. D. Lou, Steering Catalytic Activity and Selectivity of CO_2 Photoreduction to Syngas with Hydroxy-Rich Cu2S@ROH-NiCo2O3 Double-Shelled Nanoboxes, *Angew. Chem., Int. Ed.*, 2022, e202205839.

41 S. Peng, F. Gong, L. Li, D. Yu, D. Ji, T. Zhang, Z. Hu, Z. Zhang, S. Chou, Y. Du and S. Ramakrishna, Necklace-like Multishelled Hollow Spinel Oxides with Oxygen Vacancies for Efficient Water Electrolysis, *J. Am. Chem. Soc.*, 2018, **140**, 13644–13653.

42 W. Li, J. Liu, P. Guo, H. Li, B. Fei, Y. Guo, H. Pan, D. Sun, F. Fang and R. Wu, Co/CoP Heterojunction on Hierarchically Ordered Porous Carbon as a Highly Efficient Electrocatalyst for Hydrogen and Oxygen Evolution, *Adv. Energy Mater.*, 2021, **11**, 104547.

43 Y.-L. Wu, X. Li, Y.-S. Wei, Z. Fu, W. Wei, X.-T. Wu, Q.-L. Zhu and Q. Xu, Ordered Macroporous Superstructure of Nitrogen-Doped Nanoporous Carbon Implanted with Ultrafine Ru Nanoclusters for Efficient pH-Universal Hydrogen Evolution Reaction, *Adv. Mater.*, 2021, **33**, 2006965.

44 Y. Chao, P. Zhou, J. Lai, W. Zhang, H. Yang, S. Lu, H. Chen, K. Yin, M. Li, L. Tao, C. Shang, M. Tong and S. Guo, Ni1-xCoxSe$_2$-C/ZnIn_2S_4 Hybrid Nanocages with Strong 2D/2D Hetero-Interface Interaction Enable Efficient H_2-Releasing Photocatalysis, *Adv. Funct. Mater.*, 2021, **31**, 2100923.

45 Y. Huang, S. L. Zhang, X. F. Lu, Z.-P. Wu, D. Luan and X. W. Lou, Trimetallic Spinel $NiCo_{2-x}Fe_xO_4$ Nanoboxes for Highly Efficient Electrocatalytic Oxygen Evolution, *Angew. Chem., Int. Ed.*, 2021, **60**, 11841–11846.

46 H. Chen, Z. Shen, Z. Pan, Z. Kou, X. Liu, H. Zhang, Q. Gu, C. Guan and J. Wang, Hierarchical Micro-Nano Sheet Arrays of Nickel-Cobalt Double Hydroxides for High-Rate Ni-Zn Batteries, *Adv. Sci.*, 2019, **6**, 1802002.

47 C. Liu, J. Wang, J. Wan, Y. Cheng, R. Huang, C. Zhang, W. Hu, G. Wei and C. Yu, Amorphous Metal-Organic Framework-Dominated Nanocomposites with Both Compositional and Structural Heterogeneity for Oxygen Evolution, *Angew. Chem., Int. Ed.*, 2020, **59**, 3630–3637.

48 D. Feng, P. Wang, R. Qin, W. Shi, L. Gong, J. Zhu, Q. Ma, L. Chen, J. Yu, S. Liu and S. Mu, Flower-Like Amorphous MoO_{3-x} Stabilized Ru Single Atoms for Efficient Overall Water/Seawater Splitting, *Adv. Sci.*, 2023, **18**, 2300342.

49 Y.-Y. Li, B.-X. Zhou, H.-W. Zhang, T. Huang, Y.-M. Wang, W.-Q. Huang, W. Hu, A. Pan, X. Fan and G.-F. Huang, A host-guest self-assembly strategy to enhance π-electron densities in ultrathin porous carbon nitride nanocages toward highly efficient hydrogen evolution, *Chem. Eng. J.*, 2022, **430**, 132880.

50 Y.-Y. Li, Y. Si, B.-X. Zhou, W.-Q. Huang, W. Hu, A. Pan, X. Fan and G.-F. Huang, Strategy to boost catalytic activity of polymeric carbon nitride: synergistic effect of controllable *in situ* surface engineering and morphology, *Nanoscale*, 2019, **11**, 16393–16405.

51 C. Guan, X. Liu, W. Ren, X. Li, C. Cheng and J. Wang, Rational Design of Metal-Organic Framework Derived Hollow $NiCo_2O_4$ Arrays for Flexible Supercapacitor and Electrocatalysis, *Adv. Energy Mater.*, 2017, **7**, 1602391.

52 D. Zhou, S. Wang, Y. Jia, X. Xiong, H. Yang, S. Liu, J. Tang, J. Zhang, D. Liu, L. Zheng, Y. Kuang, X. Sun and B. Liu, NiFe Hydroxide Lattice Tensile Strain: Enhancement of Adsorption of Oxygenated Intermediates for Efficient Water Oxidation Catalysis, *Angew. Chem., Int. Ed.*, 2019, **58**, 736–740.

53 H. Sun, L. Chen, Y. Lian, W. Yang, L. Lin, Y. Chen, J. Xu, D. Wang, X. Yang, M. H. Rummerli, J. Guo, J. Zhong, Z. Deng, Y. Jiao, Y. Peng and S. Qiao, Topotactically

Transformed Polygonal Mesopores on Ternary Layered Double Hydroxides Exposing Under-Coordinated Metal Centers for Accelerated Water Dissociation, *Adv. Mater.*, 2020, **32**, 2006784.

54 S. L. Zhang, B. Y. Guan, X. F. Lu, S. Xi, Y. Du and X. W. Lou, Metal Atom-Doped Co_3O_4 Hierarchical Nanoplates for Electrocatalytic Oxygen Evolution, *Adv. Mater.*, 2020, **32**, 2002235.

55 Z. Zhang, X. Li, C. Zhong, N. Zhao, Y. Deng, X. Han and W. Hu, Spontaneous Synthesis of Silver-Nanoparticle-Decorated Transition-Metal Hydroxides for Enhanced Oxygen Evolution Reaction, *Angew. Chem., Int. Ed.*, 2020, **59**, 7245–7250.